22 Konig J, Cui Y, Nies AT, Keppler D. A novel human organic anion transporting polypeptide localized to the basolateral hepatocyte membrane. *Am J Physiol Gastrointest Liver Physiol* 2000; **278**: G156–64.
23 Konig J, Cui Y, Nies AT, Keppler D. Localization and genomic organization of a new hepatocellular organic anion transporting polypeptide. *J Biol Chem* 2000; **275**: 23161–8.
24 Cui Y, Konig J, Leier I, Buchholz U, Keppler D. Hepatic uptake of bilirubin and its conjugates by the human organic anion transporter SLC21A6. *J Biol Chem* 2001; **276**: 9626–30.
25 Briz O, Serrano MA, MacIas RI, Gonzalez-Gallego J, Marin JJ. Role of organic anion-transporting polypeptides, OATP-A, OATP-C and OATP-8, in the human placenta–maternal liver tandem excretory pathway for foetal bilirubin. *Biochem J* 2003; **371**: 897–905.
26 Abe T, Unno M, Onogawa T *et al.* LST-2, a human liver-specific organic anion transporter, determines methotrexate sensitivity in gastrointestinal cancers. *Gastroenterology* 2001; **120**: 1689–99.
27 Zelcer N, Reid G, Wielinga P *et al.* Steroid and bile acid conjugates are substrates of human multidrug-resistance protein (MRP) 4 (ATP-binding cassette C4). *Biochem J* 2003; **371**: 361–7.
28 Kang TW, Kim HJ, Ju H *et al.* Genome-wide association of serum bilirubin levels in Korean population. *Hum Mol Genet* 2010; **19**: 3672–8.
29 Sanna S, Busonero F, Maschio A *et al.* Common variants in the SLCO1B3 locus are associated with bilirubin levels and unconjugated hyperbilirubinemia. *Hum Mol Genet* 2009; **18**: 2711–8.
30 Narita M, Hatano E, Arizono S *et al.* Expression of OATP1B3 determines uptake of Gd-EOB-DTPA in hepatocellular carcinoma. *J Gastroenterol* 2009; **44**: 793–8.
31 Kitao A, Zen Y, Matsui O *et al.* Hepatocellular carcinoma: signal intensity at gadoxetic acid-enhanced MR Imaging – correlation with molecular transporters and histopathologic features. *Radiology* 2010; **256**: 817–26.
32 Tsuboyama T, Onishi H, Kim T *et al.* Hepatocellular carcinoma: hepatocyte-selective enhancement at gadoxetic acid-enhanced MR imaging – correlation with expression of sinusoidal and canalicular transporters and bile accumulation. *Radiology* 2010; **255**: 824–33.
33 Zucker SD, Goessling W, Ransil BJ, Gollan JL. Influence of glutathione S-transferase B (ligandin) on the intermembrane transfer of bilirubin. Implications for the intracellular transport of nonsubstrate ligands in hepatocytes. *J Clin Invest* 1995; **96**: 1927–35.
34 Smith NF, Acharya MR, Desai N, Figg WD, Sparreboom A. Identification of OATP1B3 as a high-affinity hepatocellular transporter of paclitaxel. *Cancer Biol Ther* 2005; **4**: 815–8.
35 Libra A, Fernetti C, Lorusso V *et al.* Molecular determinants in the transport of a bile acid-derived diagnostic agent in tumoral and nontumoral cell lines of human liver. *J Pharmacol Exp Ther* 2006; **319**: 809–17.
36 Ieiri I, Higuchi S, Sugiyama Y. Genetic polymorphisms of uptake (OATP1B1, 1B3) and efflux (MRP2, BCRP) transporters: implications for inter-individual differences in the pharmacokinetics and pharmacodynamics of statins and other clinically relevant drugs. *Expert Opin Drug Metab Toxicol* 2009; **5**: 703–29.

Jpn J Radiol (2011) 29:739–743
DOI 10.1007/s11604-011-0624-4

CASE REPORT

Ring-like enhancement of focal nodular hyperplasia with hepatobiliary-phase Gd-EOB-DTPA-enhanced magnetic resonance imaging: radiological-pathological correlation

Hiroyasu Fujiwara · Shigeki Sekine · Hiroaki Onaya
Kazuaki Shimada · Rintaro Mikata · Yasuaki Arai

Received: May 8, 2011 / Accepted: July 7, 2011

Abstract
We report a case of focal nodular hyperplasia in a patient for whom gadolinium-ethoxybenzyl-diethylenetriamine pentaacetic acid (Gd-EOB-DTPA)-enhanced magnetic resonance imaging (MRI) and histological analysis results were available. Dynamic contrast-enhanced computed tomography showed a well-defined hypervascular lesion 14 mm in diameter with no visible central scars. Gd-EOB-DTPA-enhanced MRI demonstrated strong peripheral enhancement of the lesion during the hepatobiliary phase, resulting in ring-like enhancement. The pathology examination revealed that the lesion was focal nodular hyperplasia (FNH). Immunohistochemistry showed positive expression of OATP8 in the hepatocytes in the peripheral areas of the lesion, whereas expression of OATP8 was lacking in hepatocytes surrounding the central radiating scar. Ring-like enhancement during the hepatobiliary phase of Gd-EOB-DTPA-enhanced MRI may be an important clue for the diagnosis of small FNH.

Key words Focal nodular hyperplasia · MRI · Gd-EOB-DTPA · Organic anion transporter

H. Fujiwara · H. Onaya (✉) · Y. Arai
Diagnostic Radiology Division, National Cancer Center Hospital, 5-1-1 Tsukiji, Chuo-ku, Tokyo 104-0045, Japan
Tel. +81-3-3542-2511; Fax +81-3-3547-5013
e-mail: honaya@ncc.go.jp

S. Sekine
Pathology Division, National Cancer Center Research Institute, Tokyo, Japan

H. Onaya
Diagnostic Radiology Section, Medical Support and Partnership Division, Center for Cancer Control and Information Services, National Cancer Center, Tokyo, Japan

K. Shimada
Hepatobiliary and Pancreatic Surgery Division, National Cancer Center Hospital, Tokyo, Japan

R. Mikata
Department of Medicine and Clinical Oncology, Graduate School of Medicine, Chiba University, Chiba, Japan

Introduction

Focal nodular hypoplasia (FNH) is a common benign lesion of the liver. Because FNH has no malignant potential, surgical intervention is not required when a diagnosis is made clinically. Radiographic imaging plays a central role in the diagnosis of FNH, and the characteristic radiological findings of FNH on computed tomography (CT) and magnetic resonance imaging (MRI) have been well documented.[1,2] However, the distinction of FNH from other hypervascular hepatic lesions is sometimes difficult, particularly in cases with atypical radiological findings or small lesions. Herein, we present a case with FNH that exhibited a peculiar radiographic finding during a Gd-EOB-DTPA-enhanced MRI examination, especially focusing on the spatial correlation between the areas of Gd-EOB-DTPA enhancement and the distribution of the expression of a hepatic uptake transporter, OATP8, in FNH.

Case report

A 36-year-old man with no remarkable past medical history was referred to our institution for further evaluation of a 14-mm focal nodular lesion in the liver. The

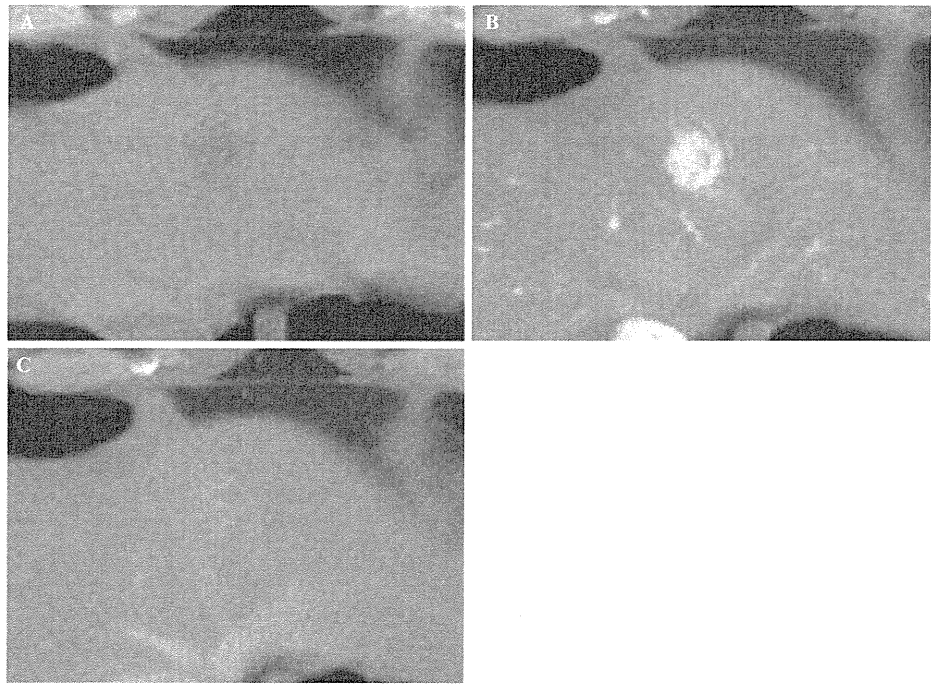

Fig. 1. Dynamic contrast-enhanced computed tomography (CT). **A** Unenhanced CT shows a slightly hypoattenuating hepatic nodule. **B** Lesion is strongly enhanced during the arterial phase of dynamic contrast-enhanced CT. **C** In the equilibrium phase, the lesion is almost isoattenuating relative to the surrounding liver without corona enhancement

lesion was incidentally found in segment 4 during an abdominal ultrasonography examination performed as part of a health checkup. His liver function was normal, and serological tests for hepatitis B and C were negative. Physicians at the previous hospital had considered the possibility of hepatocellular carcinoma (HCC) based on CT scans and MRI findings and had performed a needle biopsy. The pathological diagnosis of the biopsy specimen was suggestive of a well-differentiated HCC.

An unenhanced CT image showed a slightly hypoattenuating lesion relative to the surrounding liver (Fig. 1A). An arterial phase contrast-enhanced CT image demonstrated strong heterogeneous enhancement (Fig. 1B). An equilibrium phase contrast-enhanced CT examination showed that the lesion was almost isoattenuated relative to the surrounding liver (Fig. 1C). A central scar was not clearly seen in any phase of the CT scans.

The abdominal MRI scan was performed using a 1.5-T unit (Intera Achieva; Philips Medical Systems, Best, The Netherlands). The lesion was hypointense on T1-weighted images and inhomogeneously hyperintense on T2-weighted images (Fig. 2A,B). After the administration of Gd-EOB-DTPA (Primovist; Bayer HealthCare, Osaka, Japan), the lesion showed marked heterogeneous enhancement during the arterial phase, similar to the results obtained using dynamic contrast-enhanced CT (Fig. 2C). During the hepatobiliary phase, the lesion showed ring-like enhancement, with peripheral uptake of Gd-EOB-DTPA (Fig. 2D). Because the possibility of malignancy could not be excluded based on these radiological findings, the lesion was removed during a partial segmentectomy.

The pathological diagnosis of the surgically resected specimen was FNH. The lesion was well demarcated and had a central radial scar (Fig. 3A). The central scar was not well developed and consisted of thin, fibrous septa containing vessels and bile ducts. Immunohistochemistry for hepatocyte-specific antigen indicated that most areas of the FNH, except the thin, radial, fibrous septa, consisted of hepatocytes (Fig. 3B). The hepatocytes in the peripheral areas of the lesion exhibited strong OATP8 expression, whereas the hepatocytes in the central areas, surrounding the thin radial scars, were negative for it (Fig. 3C,D). In the liver tissue surrounding the lesion, OATP8 was expressed in the pericentral hepatocytes.

Discussion

The typical MRI findings for FNH are homogeneous isointensity or slight hypointensity on T1-weighted images and isointensity or slight hyperintensity on T2-weighted images.[1,2] The central scar appears as a hyperintense area on T2-weighted images.[1,2] Because the lesion in our case showed inhomogeneous hyperintensity without a central scar on T2-weighted images, these findings obtained using unenhanced MRI did not allow a

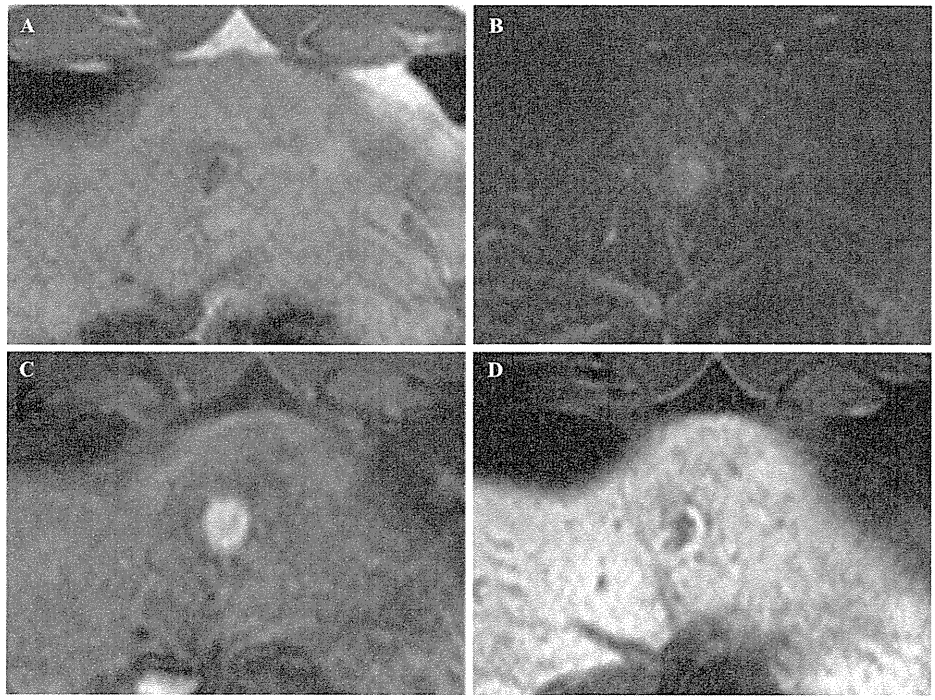

Fig. 2. Gadolinium-ethoxybenzyl-diethylenetriamine pentaacetic acid (Gd-EOB-DTPA)-enhanced magnetic resonance imaging (MRI). **A** On unenhanced T1-weighted imaging (TR/TE 4.0/2.1), the nodular lesion appears as central hypointensity with peripheral isointensity. **B** T2-weighted MRI (TR/effective TE 2000/100) shows inhomogeneous signal intensity. **C** Arterial phase of Gd-EOB-DTPA-enhanced dynamic MRI (TR/TE 4.0/2.1) shows a well-demarcated, nearly homogeneously enhanced lesion. **D** During the hepatobiliary phase obtained 15 min after injection, the lesion exhibited ring-like enhancement, with strong enhancement of the peripheral portion that shows isointensity in **A**, the unenhanced T1-weighted image

definitive diagnosis of FNH. In some cases, particularly with small FNH (≤3 cm), the central scar may be extremely small or even undetectable on CT (61%–80%) and MRI (80%).[3]

Gd-EOB-DTPA, an increasingly used hepatobiliary-specific contrast agent for MRI, is actively taken up by hepatocytes and excreted into bile. Hepatobiliary-specific agents are particularly useful for determining whether a lesion is of hepatocellular origin.[3,4] The characterization of FNH provided by Gd-EOB-DTPA-enhanced MRI is superior to that provided by unenhanced MRI or dynamic CT.[5] FNH shows intense enhancement similar to that of other extracellular gadolinium-based contrast agents during the arterial phase after the bolus injection of Gd-EOB-DTPA.[4,5] In the hepatobiliary phase, enhancement is regularly seen (88%–90%) as hyperintense or isointense relative to the liver.[5]

Central scars appear as hypointense areas in the hepatobiliary phase of Gd-EOB-DTPA-enhanced MRI.[4,6,7] On the other hand, central scars show delayed enhancement on MRI when using other extracellular fluid gadolinium-based contrast agents.[6,7] However, previous reports have not examined the precise radiological–pathological correlation; their observations were mainly based on comparisons of radiological findings using various modalities with different contrast materials. The present FNH lesion showed a central hypointense area with peripheral hyperintensity in the hepatobiliary phase of Gd-EOB-DTPA-enhanced MRI. As mentioned above, however, the central scar in this case could not be detected on either CT or MRI. Indeed, the pathological features agreed with the findings of dynamic CT and unenhanced MRI; the central radial scar consisted of thin, fibrous septa and was not well developed. Taken together, the presence of the central scar does not explain the hypointense area that was observed in the center of this lesion during the hepatobiliary phase.

OATP8 is a member of the solute carrier organic anion transporter family and is specifically expressed at the basolateral membrane of hepatocytes. Expression of OATP8 is associated with uptake of Gd-EOB-DTPA in HCCs.[8,9] Interestingly, the present lesion exhibited strong expression of OATP8 in peripheral areas of the lesion, consistent with a previous report.[10]

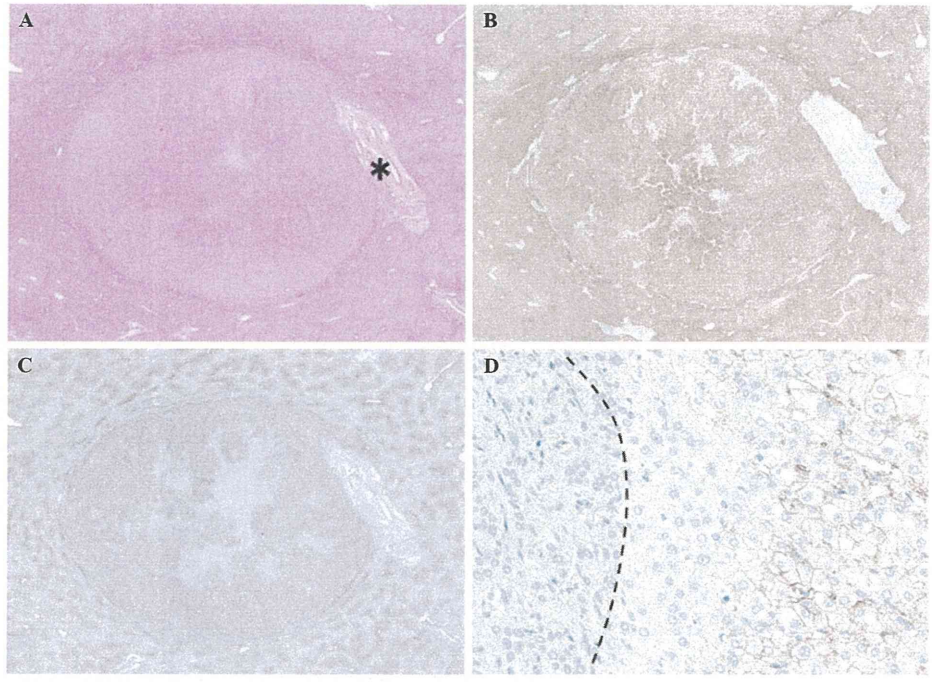

Fig. 3. Histological and immunohistochemical findings. **A** Histology of the lesion. Focal nodular hypoplasia (FNH) is well demarcated and has a central radial scar. A large portal tract (*asterisk*) is located adjacent to the lesion (H&E). **B** Immunohistochemistry (IHC) for hepatocyte-specific antigen. Most FNH areas show positive staining, indicating that the lesion is mostly composed of hepatocytes. Radial fibrous scars in the lesion and portal tracts in surrounding liver tissue are visible as nonstained areas. **C** IHC for OATP8. Peripheral portion of the lesion strongly expresses OATP8, whereas the central area is negative. Areas of OATP8-negative hepatocytes become evident when compared with the staining for hepatocyte-specific antigen (**B**). Normal liver tissue exhibits a pericentral expression pattern. **D** Magnified view of OATP8 staining in the lesion. *Dashed line* indicates the border between the fibrous scar (*left*) and hepatocytes (*right*). Hepatocytes close to the fibrous scar are negative for OATP8. Other peripheral hepatocytes exhibit membranous expression of OATP8

In the normal liver, OATP8 is expressed in pericentral hepatocytes but is absent in periportal hepatocytes.[10] Considering the fact that the central scar of FNH contains bile ducts, it is reasonable that hepatocytes surrounding the central scar do not express OATP8, similar to periportal hepatocytes. On the basis of the suggested role of OATP8 in Gd-EOB-DTPA uptake,[8,9] this distinct localization pattern of OATP8 expression (i.e., centrally negative versus peripherally positive) reasonably explains the ring-like enhancement pattern observed on Gd-EOB-DTPA-enhanced MRI. We suggest that the central hypointense area was due not only to the presence of the central scar but also to the absence of OATP8 expression in the hepatocytes surrounding the central scar. Thus, the ring-like enhancement on Gd-EOB-DTPA-enhanced MRI seems to be a diagnostic clue for small FNH, even in the presence of atypical radiological features of FNH (e.g., inhomogeneous enhancement or a missing central scar) that may cause problems in differentiating this lesion from other liver lesions. However, this finding can be observed theoretically in HCCs or hepatic adenomas with central necrosis and nodule-in-nodule-type HCC. An analysis of additional cases should help to elucidate the specificity of this finding and the differential diagnosis.

Conclusion

The presence of a ring-like enhancement during the hepatobiliary phase of Gd-EOB-DTPA-enhanced MRI may be an important radiographic feature of small FNH, regardless of the presence of central scar. The good spatial correlation between the OATP8-expressing area and the enhanced area on hepatobiliary-phase Gd-EOB-DTPA-enhanced MRI observed for the present FNH lesion further supports the role of OATP8 as a major transporter of Gd-EOB-DTPA.

Acknowledgments. We express our sincere thanks to Hidenori Ojima for valuable advice. This work was supported in part by grants-in-aid for Research on Publicly Essential Drugs and Medical Devices from the Japan Health Science Foundation and

for Cancer Research (21S-1) from the Ministry of Health, Labor, and Welfare, Japan.

References

1. Mortelé KJ, Praet M, Van Vlierberghe H, Kunnen M, Ros PR. CT and MR imaging findings in focal nodular hyperplasia of the liver: radiologic-pathologic correlation. AJR Am J Roentgenol 2000;175:687–92.
2. Ba-Ssalamah A, Schima W, Schmook MT, Linnau KF, Schibany N, Helbich T, et al. Atypical focal nodular hyperplasia of the liver: imaging features of nonspecific and liver-specific MR contrast agents. AJR Am J Roentgenol 2002;179: 1447–56.
3. Grazioli L, Morana G, Federle MP, Brancatelli G, Testoni M, Kirchin MA, et al. Focal nodular hyperplasia: morphological and functional information from MR imaging with gadobenate dimeglumine. Radiology 2001;221:731–9.
4. Huppertz A, Haraida S, Kraus A, Zech CJ, Scheidler J, Breuer J, et al. Enhancement of focal liver lesions at gadoxetic acid-enhanced MR imaging: correlation with histopathologic findings and spiral CT—initial observations. Radiology 2005;234: 468–78.
5. Zech CJ, Grazioli L, Breuer J, Reiser MF, Schoenberg SO. Diagnostic performance and description of morphological features of focal nodular hyperplasia in Gd-EOB-DTPA-enhanced liver magnetic resonance imaging: results of a multicenter trial. Invest Radiol 2008;43:504–11.
6. Kacl GM, Hagspiel KD, Marincek B. Focal nodular hyperplasia of the liver: serial MRI with Gd-DOTA, superparamagnetic iron oxide, and Gd-EOB-DTPA. Abdom Imaging 1997; 22:264–7.
7. Karam AR, Shankar S, Surapaneni P, Kim YH, Hussain S. Focal nodular hyperplasia: central scar enhancement pattern using gadoxetate disodium. J Magn Reson Imaging 2010;32: 341–4.
8. Kitao A, Zen Y, Matsui O, Gabata T, Kobayashi S, Koda W, et al. Hepatocellular carcinoma: signal intensity at gadoxetic acid-enhanced MR imaging—correlation with molecular transporters and histopathologic features. Radiology 2010;256: 817–26.
9. Tsuboyama T, Onishi H, Kim T, Akita H, Hori M, Tatsumi M, et al. Hepatocellular carcinoma: hepatocyte-selective enhancement at gadoxetic acid-enhanced MR imaging—correlation with expression of sinusoidal and canalicular transporters and bile accumulation. Radiology 2010;255:824–33.
10. Vander Borght S, Libbrecht L, Blokzijl H, Faber KN, Moshage H, Aerts R, et al. Diagnostic and pathogenetic implications of the expression of hepatic transporters in focal lesions occurring in normal liver. J Pathol 2005;207:471–82.

Carcinogenesis vol.32 no.4 pp.622–628, 2011
doi:10.1093/carcin/bgr002
Advance Access publication January 7, 2011

Hepatomas with activating *Ctnnb1* mutations in '*Ctnnb1*-deficient' livers: a tricky aspect of a conditional knockout mouse model

Shigeki Sekine*, Reiko Ogawa and Yae Kanai

Pathology Division, National Cancer Center Research Institute, 5-1-1, Tsukiji, Chuo-ku, Tokyo, Japan 104-0045

*To whom correspondence should be addressed. Tel: +81 3 3542 2511; Fax: +81 3 3248 2463;
Email: ssekine@ncc.go.jp

Conditional knockout mice, based on the Cre-loxP system, are a widely used model for examining organ-specific gene functions. To date, efficient hepatocyte-specific knockout has been reported in many different models, but little attention has been paid to the long-term stability of the recombination efficiency. In the present study, we characterized *Alb-Cre;Ctnnb1*$^{flox/flox}$ 'hepatocyte-specific *Ctnnb1* knockout' mice of different ages to test whether efficient recombination is maintained over time. At 2 months of age, the knockout mouse livers achieved efficient deletions of β-catenin in hepatocytes. However, as the mice aged, the reappearance and expansion of β-catenin-expressing hepatocytes were observed. In 1-year-old mice, a significant proportion of the pericentral hepatocytes in the knockout mouse livers were replaced with β-catenin-positive hepatocytes, whereas the periportal hepatocytes mostly remained β-catenin-negative. Furthermore, most of the 1-year-old mice spontaneously developed hepatocellular adenomas and carcinomas that were positive for β-catenin and overexpressed glutamine synthetase and Slc1a2, both of which are hallmarks of active β-catenin signaling. Sequencing analysis revealed that the *Ctnnb1* alleles were not inactivated but had activating mutations in these tumors. The present study suggests that recombination efficiency should be carefully examined when hepatocyte-specific knockout mice of different ages are analyzed. In addition, illegitimate deletion mutations should be recognized as potential adverse effects of the Cre-loxP system.

Introduction

Knockout mouse models are an important tool for investigating gene functions *in vivo*. Although systemic knockout is the most straightforward strategy, conditional knockout models based on the Cre-loxP system are also widely used when systemic knockout results in a lethal outcome or an organ-specific gene function needs to be determined (1,2). Several Cre transgenic lines have been generated to achieve the hepatocyte-specific recombination of conditional alleles. Among them, *Alb-Cre* mice are widely used to achieve recombination in the adult liver, and the use of this strain reportedly allows the virtually complete deletion of conditional alleles in adult hepatocytes (3,4).

β-Catenin, encoded by *Ctnnb1*, is involved in two distinct processes in cells: cell adhesion and the transduction of Wnt signaling. In the absence of active Wnt signaling, β-catenin is mostly localized to the membrane in a complex with cadherins that mediates cell–cell adhesion. When the Wnt signaling pathway is activated, β-catenin accumulates in the cytoplasm and translocates to the nucleus, where it activates T cell factor (TCF)-dependent transcription (5). Recent studies have revealed multiple physiological roles of β-catenin in hepatocytes, including the regulation of metabolism and proliferation. In addition to these physiologic functions, β-catenin also plays a role in tumorigenesis. The acquisition of oncogenic *Ctnnb1* mutations leads to constitutively active TCF-dependent transcription, and the dysregulated expression of β-catenin/TCF target genes is thought to promote tumorigenesis (6). Oncogenic *CTNNB1* mutations have been identified in a variety of human tumors, and ~30% of hepatocellular carcinomas harbor *CTNNB1* mutations (7,8).

We previously generated *Alb-Cre;Ctnnb1*$^{flox/flox}$ mice, in which β-catenin was efficiently eliminated from adult hepatocytes, to examine the functions of β-catenin in the liver (9,10). However, we noted that the efficient disruption of β-catenin was not stably maintained: the mutant livers were gradually repopulated with wild-type hepatocytes as the mice aged. Furthermore, the majority of 1-year-old mice unexpectedly developed hepatocellular adenomas and carcinomas. Our observations revealed some critical adverse effects of the Cre-loxP system in hepatocyte-specific knockout models.

Abbreviations: PCR, polymerase chain reaction; RT, reverse transcription; TCF, T cell factor.

Materials and methods

Mice

Alb-Cre (3,4), *Ctnnb1*$^{flox/flox}$ (11) and *Alb-Cre;Ctnnb1*$^{flox/flox}$ (10) mice were on a C57 background and generated as described previously. The mice used in the present study were maintained in barrier facilities according to the protocols approved by the Committee for Ethics in Animal Experimentation at the National Cancer Center, Japan.

Reverse transcription–polymerase chain reaction

RNA extraction, reverse transcription (RT) and conventional polymerase chain reaction (PCR) were performed using standard protocols (12). For conventional PCR, the PCR products were electrophoresed in an agarose gel and visualized under ultraviolet light with ethidium bromide staining. Quantitative RT–PCR reactions were performed using FastStart Universal Probe Master (Roche Applied Science, Penzberg, Germany). The expression level of each gene was determined using *Gusb* as a standard, as described previously (10). The primer sequences and probes used in the present study are shown in supplementary Table 1, available at *Carcinogenesis* Online.

Histology and immunohistochemistry

Liver tissue samples were fixed in 10% buffered formalin and embedded in paraffin; sections were then subjected to hematoxylin and eosin and immunohistochemical staining. Immunohistochemistry was performed using an indirect immunoperoxidase method with peroxidase-labeled anti-mouse, anti-rabbit or anti-rat polymers (Histofine Simple Stain; Nichirei, Tokyo, Japan), as described previously (13). The primary antibodies used in the present study were anti-β-catenin (clone 14; 1:250 dilution; BD Bioscience, San Diego, CA), anti-Cyp2e1 (polyclonal, 1:1000 dilution; gift from Dr Magnus Ingelman-Sundberg), anti-GLT-1 (polyclonal, 1:500 dilution; gift from Masahiko Watanabe), anti-glutamine synthetase (clone 6; 1:500 dilution; Becton Dickinson, Franklin Lakes, NJ) and anti-Ki-67 (clone TEC-3; 1:200 dilution; DAKO, Glostrup, Denmark).

Double immunohistochemical staining was performed using glycine buffer treatment following the first antibody reaction as described previously (14). 3,3′-Diaminobenzidine tetrahydrochloride and Vector VIP (Vector Laboratories, Burlingame, CA) were used as chromogens.

Mutational analysis

Paraffin embedded or frozen tissue samples were used for DNA extraction. The samples were incubated in a DNA extraction buffer (50 mmol/l Tris–HCl, pH 8.0, 1 mmol/l ethylenediaminetetraacetic acid, 0.5% (vol/vol) Tween 20, 200 μg/ml proteinase K) at 55°C overnight. Proteinase K was inactivated by heating at 100°C for 10 min. The digested DNA samples were directly subjected to PCR (15). Complementary DNA samples, prepared as described above, were also used for sequencing analysis. The primers used for the mutational analysis are listed in supplementary Table 2, available at *Carcinogenesis* Online. The PCR products were electrophoresed in an agarose gel, visualized under ultraviolet light with ethidium bromide staining and recovered using a QIAquick Gel Extraction Kit (Qiagen Hilden, Germany). When PCR products of different sizes were detected, they were separately isolated. Isolated PCR products were sequenced bidirectionally using the same primers that were used for amplification.

Western blotting

Tissue samples were homogenized in Radioimmunoprecipitation assay buffer [50 mM Tris–HCl, pH 7.4, 1% (vol/vol) NP40, 0.1% (wt/vol) sodium dodecyl

sulfate, 0.25% (wt/vol) Na-deoxycholate and 1 mM ethylenediaminetetraacetic acid] with protease inhibitors (Complete; Roche Applied Science). Equal amounts of proteins were electrophoresed on 10% sodium dodecyl sulfate–polyacrylamide electrophoresis gels and transferred to a polyvinylidene difluoride membrane, then processed for immunoblotting with antibodies for β-catenin (clone 14; 1:2000 dilution) and glutamine synthetase (clone 6; 1:5000 dilution). Horseradish peroxidase-conjugated anti-mouse secondary antibody was used at a dilution of 1:5000 and was detected using enhanced chemiluminescence (GE Healthcare, Pittsburg, CA). The protein-transferred membrane was stained with Coomassie brilliant blue as a loading control.

Statistical analysis

The results are presented as the mean ± standard deviation. *P* value of <0.05 by Student's two-tailed t test was considered to be significant.

Results

Efficient disruption of β-catenin in Alb-Cre;Ctnnb1$^{flox/flox}$ mouse livers is not maintained in elderly mice

We previously showed that young adult *Alb-Cre;Ctnnb1$^{flox/flox}$* mouse livers exhibited the efficient disruption of *Ctnnb1* in hepatocytes (9,10). However, whether efficient recombination was stably maintained over a long time period was unclear. To test this issue, we used quantitative RT–PCR to examine the expression of *Ctnnb1* in the livers of 2-, 4-, 8- and 12-month-old *Alb-Cre;Ctnnb1$^{flox/flox}$* mice. In the 2-month-old *Alb-Cre;Ctnnb1$^{flox/flox}$* mice, the expression of *Ctnnb1* was reduced to 10% of that in the controls (Figure 1A). *Ctnnb1* expression was repressed to a similar level in the 4-month-old mice but significantly recovered in the 8- and 12-month-old mice. Although the repression of *Ctnnb1* was not complete even in the 2-month-old mice, this effect was probably due to the presence of a non-parenchymal cell population that retained *Ctnnb1* expression (10).

To estimate the recombination efficiency of *Ctnnb1* alleles specifically in hepatocytes, we also quantified the expressions of *Glul* and *Cyp2e1* (Figure 1B and C). These two genes are exclusively expressed in hepatocytes in the liver and their expressions require β-catenin (10). Although the expressions of *Glul* and *Cyp2e1* were almost completely diminished in the 2-month-old mutant mice, the expressions gradually recovered as the mice aged. In the 1-year-old mice, the *Glul* and *Cyp2e1* expression levels were about a quarter of that observed in the controls. These findings indicated that the *Ctnnb1* alleles were efficiently deleted in the hepatocytes of 2-month-old *Alb-Cre;Ctnnb1$^{flox/flox}$* mice, but that this deletion efficiency was not stably maintained over a long time period.

β-Catenin-positive hepatocytes repopulate pericentral areas of elderly Alb-Cre;Ctnnb1$^{flox/flox}$ mouse livers

We next performed immunohistochemistry to determine the localization of β-catenin (encoded by *Ctnnb1*)-positive hepatocytes in these mice. Control mouse livers exhibited the membranous expression of β-catenin in hepatocytes (Figure 2A). In contrast, the 2-month-old *Alb-Cre;Ctnnb1$^{flox/flox}$* mouse livers exhibited the virtually complete loss of β-catenin in the hepatocytes, whereas the sinusoidal endothelial cells retained β-catenin expression (Figure 2D). In the 4-month-old *Alb-Cre;Ctnnb1$^{flox/flox}$* mice, a few β-catenin-positive hepatocytes were detected (Figure 2G). The β-catenin-positive hepatocytes had expanded and formed clusters in the 8-month-old mice (Figure 2J); in the 12-month-old mice, the β-catenin-positive hepatocytes had predominantly repopulated the pericentral areas within the liver lobules, whereas the periportal areas mostly remained negative for β-catenin (Figure 2M).

Immunohistochemistry for two β-catenin-regulated gene products, glutamine synthetase (encoded by *Glul*) and Cyp2e1, produced findings that were consistent with β-catenin immunohistochemistry results. In the control mice, glutamine synthetase was expressed in a few layers of hepatocytes surrounding the central veins (Figure 2B), whereas Cyp2e1 was expressed in broader pericentral areas (Figure 2C). In the 2-month-old *Alb-Cre;Ctnnb1$^{flox/flox}$* mice, the expressions of glutamine synthetase and Cyp2e1 were detected only in a few hepatocytes in the liver (Figure 2E and F). A small, but increased number of glutamine synthetase- and Cyp2e1-positive hepatocytes appeared in the 4-month-old mice (Figure 2H and I), and this cell population had further expanded in the 8-month-old mice (Figure 2K and L). In the 12-month-old mice, the pericentral expression patterns of these proteins were readily recognizable (Figure 2N and O). Interestingly, in 2–8-month-old mice, some glutamine synthetase- and Cyp2e1-positive hepatocytes were also observed in periportal areas, consistent with a finding reported by Braeuning *et al.*. (16). However, these cells were mostly localized to pericentral areas in 12-month-old mice.

Since the number of β-catenin-expressing hepatocytes increased with age, we assumed that these cells had a growth advantage over β-catenin-deficient hepatocytes. To test this hypothesis, we quantified the numbers of proliferating hepatocytes in β-catenin-positive and-deficient cell populations using immunohistochemistry for Ki-67. As a result, the proliferation of β-catenin-positive hepatocytes in *Alb-Cre;Ctnnb1$^{flox/flox}$* mice was significantly increased proliferation, compared with the proliferation of β-catenin-deficient hepatocytes and hepatocytes in wild-type mice (Figure 3). Since β-catenin-deficient hepatocytes were replaced by β-catenin-positive hepatocytes over time, we suspected that the β-catenin-deficient hepatocytes might be lost to apoptosis. However, we did not observe a significant

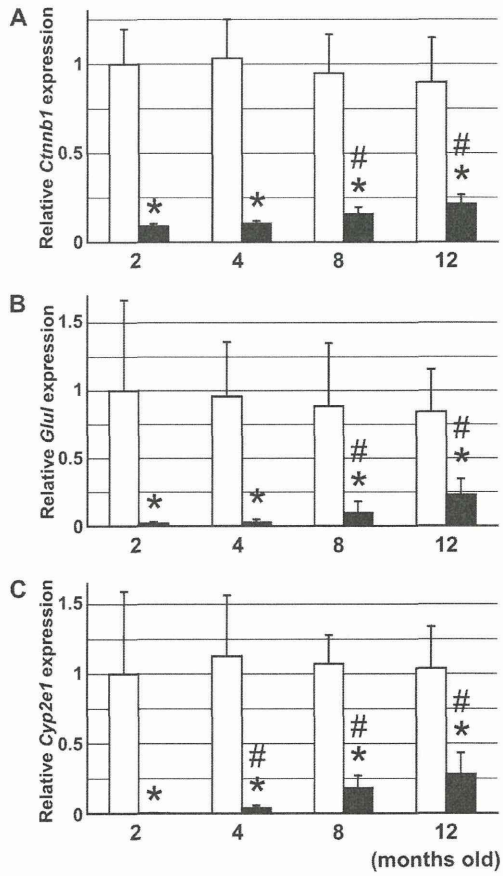

Fig. 1. Expression of *Ctnnb1*, *Glul* and *Cyp2e1* in *Alb-Cre;Ctnnb1$^{flox/flox}$* mouse livers at different ages. The expression levels of *Ctnnb1* (**A**), *Glul* (**B**) and *Cyp2e1* (**C**) in livers of *Alb-Cre;Ctnnb1$^{flox/flox}$* and control *Ctnnb1$^{flox/flox}$* mouse livers of different ages were determined using quantitative RT–PCR. White bars: controls; Black bars: *Alb-Cre;Ctnnb1$^{flox/flox}$* mice. n = 6–9 per group. Values are presented as the means ± standard deviations. $^{*}P < 0.05$ compared with controls of the same age. $\#P < 0.05$ compared with 2-month-old mice of the same genotype.

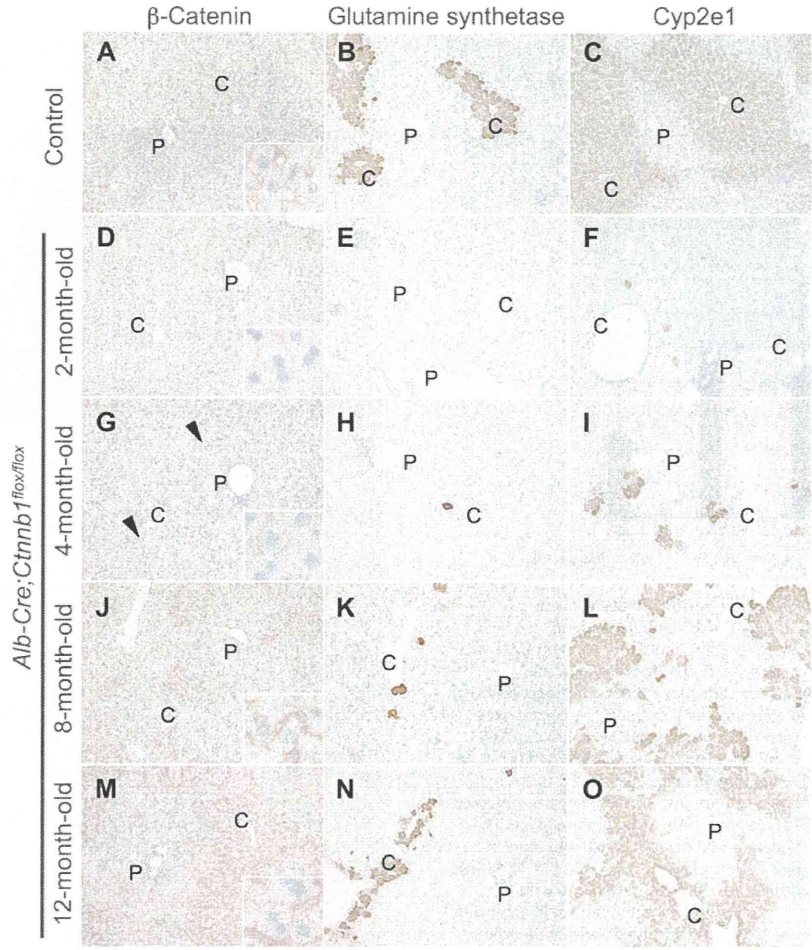

Fig. 2. Expression of β-catenin, glutamine synthetase and Cyp2e1 in *Alb-Cre;Ctnnb1*$^{flox/flox}$ mouse livers at different ages. Expressions of β-catenin (**A**, **D**, **G**, **J** and **M**), glutamine synthetase (**B**, **E**, **H**, **K** and **N**) and Cyp2e1 (**C**, **F**, **I**, **L** and **O**) in control (A–C) and *Alb-Cre;Ctnnb1*$^{flox/flox}$ mouse livers (D–O), as determined using immunohistochemistry. Insets show high-magnification views of β-catenin staining (A, D, G, J and M). A few β-catenin-positive hepatocytes are indicated by the arrowheads (G). At least four mice were examined per group and representative results are presented. C, central veins; P, portal veins.

elevation in apoptotic activity in β-catenin-deficient hepatocytes using a TUNEL assay or immunohistochemistry for cleaved caspase-3 (data not shown), although an increase in apoptosis might not have been detectable because the replacement process progressed very slowly over a period of months.

Together, these results indicate that the β-catenin is efficiently eliminated in 2-month-old *Alb-Cre;Ctnnb1*$^{flox/flox}$ mouse hepatocytes; however, a gradual repopulation with β-catenin-positive hepatocytes occurred in older mice. This process is achieved through the expansion of a few residual β-catenin-positive hepatocytes in young *Alb-Cre;Ctnnb1*$^{flox/flox}$ mouse livers. Notably, β-catenin-positive hepatocytes predominantly repopulated the pericentral areas within the liver lobules in elderly mice, suggesting that the retention of wild-type β-catenin confers survival advantages to hepatocytes in the pericentral areas within the liver lobule.

Development of hepatocellular adenomas and carcinomas in Alb-Cre;Ctnnb1$^{flox/flox}$ *mouse livers*

Unexpectedly, we noted that 11 of the 13 *Alb-Cre;Ctnnb1*$^{flox/flox}$ mice used in this study spontaneously developed liver tumors at an age of 1 year (Figure 4A). Most of the mice had one to five tumors, but two mice developed numerous tumors involving almost the entire liver. Among the tumors that were histologically examined, 17 lesions were hepatocellular adenomas and consisted of tumor cells without apparent atypia arranged in thin trabecule (Figure 4B and C; supplementary Table 3 is available at *Carcinogenesis* Online) (17). Eight lesions showed significant structural and/or cytological atypia enabling a diagnosis of hepatocellular carcinoma (Figure 4D). Surprisingly, immunohistochemistry demonstrated the membranous expression of β-catenin in 24 of the 25 tumors, including both adenomas and carcinomas (Figure 4E). Among these, 10 lesions also exhibited the nuclear and cytoplasmic accumulation of β-catenin (Figure 4F). Furthermore, all the β-catenin-positive tumors expressed glutamine synthetase and Slc1a2, which are hallmarks of active Wnt/β-catenin signaling (Figure 4G and H) (18,19), regardless of the presence of the nuclear/cytoplasmic accumulation of β-catenin. β-Catenin, glutamine synthetase and Slc1a2 were not expressed in one adenoma (Figure 4I and J).

Tumors developed in Alb-Cre;Ctnnb1$^{flox/flox}$ *mouse livers harbor activating Ctnnb1 mutations*

The expression of glutamine synthetase and Slc1a2 in a hepatocellular tumor implies the presence of active Wnt/β-catenin signaling in these tumors. Since genetic alterations of *Ctnnb1* are the most common mechanism responsible for the activation of this pathway during tumorigenesis, we analyzed the presence of *Ctnnb1* gene mutations.

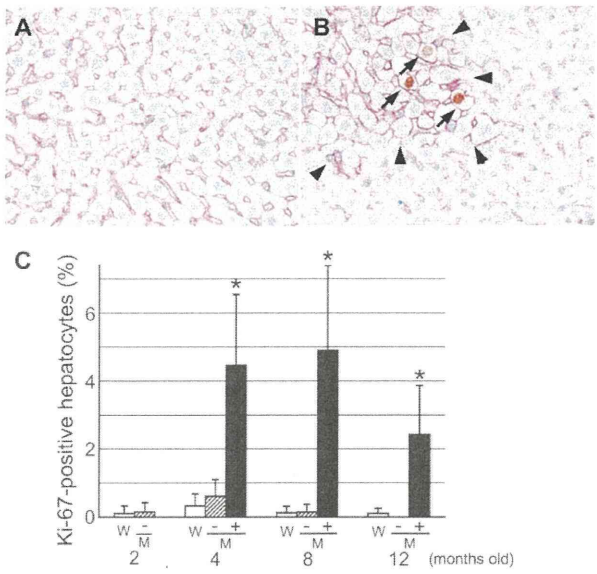

Fig. 3. Proliferative activity of β-catenin-positive hepatocytes in *Alb-Cre;Ctnnb1*$^{flox/flox}$ mouse livers (**A** and **B**) Double staining immunohistochemistry for β-catenin (purple) and Ki-67 (brown) in control (A) and *Alb-Cre;Ctnnb1*$^{flox/flox}$ mouse livers (B) from 8-month-old. Hepatocytes in the control mouse liver show the membranous expression of β-catenin, but no Ki-67-positive cells are visible (A). Three hepatocytes within a cluster of β-catenin-positive hepatocytes (arrowheads) express Ki-67 (arrows) (B). Note that the sinusoidal endothelial cells retain β-catenin expression in the areas of the β-catenin-deficient hepatocytes. (**C**) Quantitative analysis of proliferative activity. At least 300 hepatocytes were counted when analysing the Ki-67-positive cells in each population. The values are presented as the mean ± standard deviation. The numbers of β-catenin-positive hepatocytes in 2-month-old *Alb-Cre;Ctnnb1*$^{flox/flox}$ mouse livers were too small to be quantified. n = 4–6 per group. W, wild-type controls; M, *Alb-Cre;Ctnnb1*$^{flox/flox}$ mice; −, β-catenin-deficient hepatocytes; +, β-catenin-positive hepatocytes; $^{*}P < 0.05$ compared with wild-type controls of the same age.

Sequencing analyses identified deletion mutations within *Ctnnb1* in 18 of the 23 lesions that were examined (Figure 5A–E; supplementary Table 3 is available at *Carcinogenesis* Online). Of note, 10 mutations involved the first loxP site at their breakpoints. Furthermore, deletions in the messenger RNA transcripts were also identified in 13 of the 17 tumors that were examined. These deletions involved sequences encoding the N-terminal region of β-catenin, which is required for proteasomal degradation. On the other hand, analysis of messenger RNA samples of non-neoplastic tissue showed wild-type sequences of *Ctnnb1*.

Consistent with the presence of the deletion mutations, truncated protein products were identified using western blotting in all 13 samples that were examined (Figure 5F; supplementary Table 3 is available at *Carcinogenesis* Online). Even though the expression levels of truncated β-catenin were not significantly increased compared with the corresponding levels of wild-type β-catenin in non-neoplastic liver tissues, this observation is consistent with previous studies on *Ctnnb1*-mutated mouse liver tumors (20,21). The overexpression of glutamine synthetase was also confirmed using western blotting in tumors. We also examined *Cre* transgene expression in these tumors using RT–PCR and found that 15 of 18 tumors examined retained *Cre* expression (Figure 5G). Expression of *Cre* was significantly reduced in the remaining three tumors. Together, these findings suggest that most of the liver tumors in the *Alb-Cre;Ctnnb1*$^{flox/flox}$ mice-harbored *Ctnnb1* mutations that resulted in the truncation of β-catenin, and the expression of the *Cre* transgene was not silenced in most of the tumors.

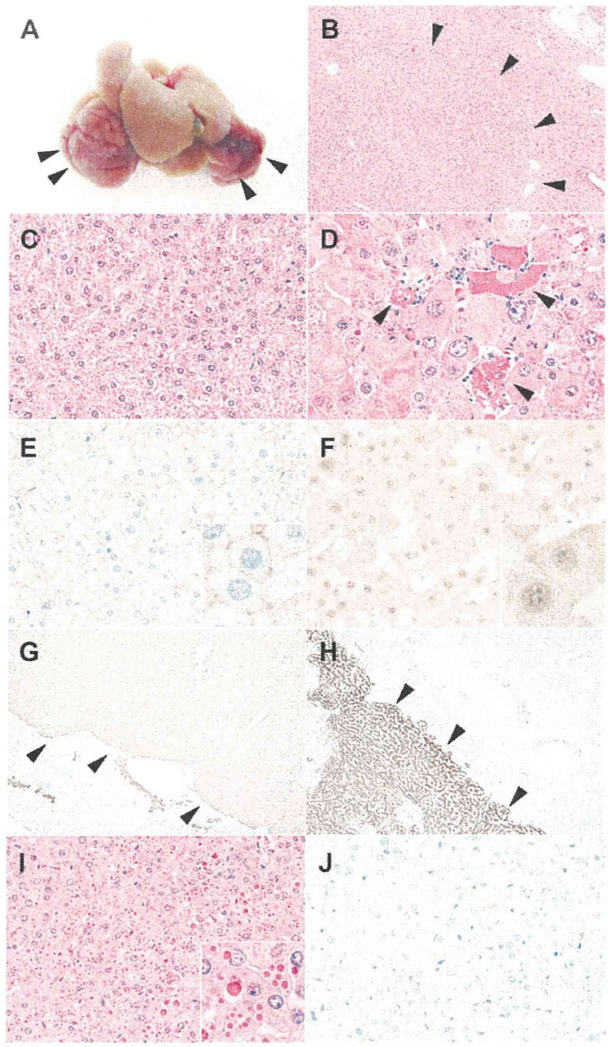

Fig. 4. Development of liver tumors in *Alb-Cre;Ctnnb1*$^{flox/flox}$ mouse livers (**A**) Gross morphology of liver tumors in a 1-year-old *Alb-Cre;Ctnnb1*$^{flox/flox}$ mouse (arrowheads). (**B**) Low power magnification of a hepatocellular adenoma exhibiting expansive growth (arrowheads). (**C**) Hepatocellular adenoma. Well-differentiated hepatocytes without apparent cellular atypia are arranged in a thin trabecular pattern. (**D**) Hepatocellular carcinoma. Tumor cells are variable in size and exhibit prominent nuclear atypia. Foci of single cell necrosis are visible (arrowheads). (**E**) Hepatocellular adenoma exhibiting membranous β-catenin expression (inset: high power magnification). (**F**) Hepatocellular adenoma showing the cytoplasmic and nuclear accumulation, in addition to membranous expression, of β-catenin (inset: high power magnification). (**G**) Expression of glutamine synthetase in a hepatocellular adenoma (arrowheads). Non-neoplastic hepatocytes surrounding the central veins are also stained positive. (**H**) Expression of Slc1a2 in a hepatocellular adenoma (arrowheads). The pericentral hepatocytes also express Slc1a2. (**I** and **J**) Histology of a β-catenin-negative adenoma. The tumor cells contain numerous hyaline globules (I, inset: high power magnification) and lack β-catenin expression (J).

Discussion

Alb-Cre transgenic mice have been widely used to achieve hepatocyte-specific recombination in adult mice (3,4). The use of this strain enables the virtually complete recombination of conditional alleles flanked by loxP sites in adult hepatocytes since the *Alb* promoter is

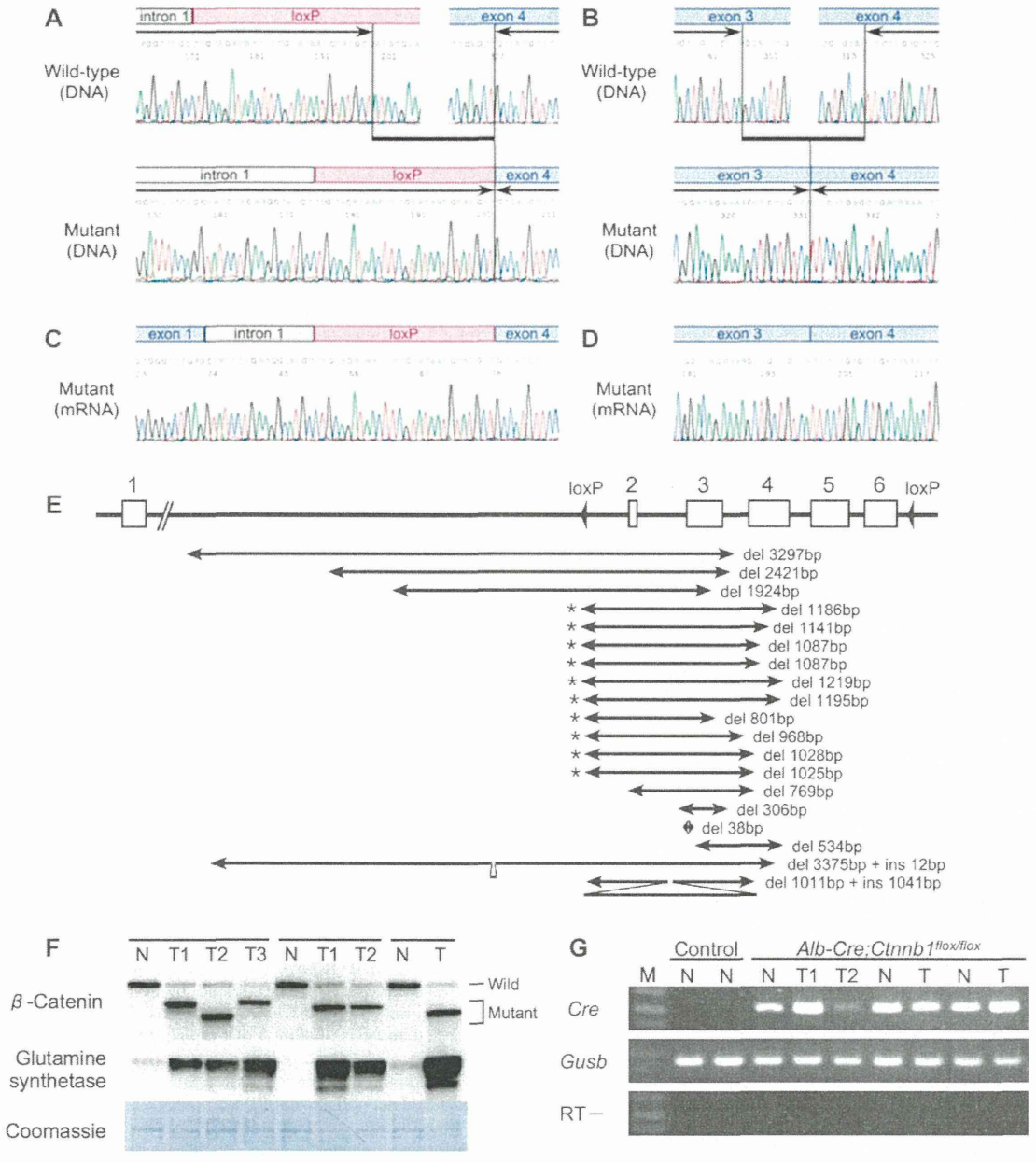

Fig. 5. Liver tumors in *Alb-Cre;Ctnnb1*$^{flox/flox}$ mice harbor *Ctnnb1* mutations (**A** and **C**) An example of a deletion mutation involving the first loxP site. The deletion mutation spans the first loxP sequence to exon 4 (A). This deletion mutation resulted in aberrant splicing and parts of intron 1 and loxP were inserted between exon 1 and a truncated exon 4 (C). (**B** and **D**) Another example of a deletion mutation spanning exons 3 and 4 (B). This deletion resulted in a 390 bp in-frame deletion at the messenger RNA level (D). (**E**) Deletion mutations in liver tumors in *Alb-Cre;Ctnnb1*$^{flox/flox}$ mice. The deletions detected in the liver tumors are indicated by the arrows. Ten of the nineteen deletions involved the first loxP site at their breakpoints (indicated by the asterisks). Two mutations were associated with insertions. Open boxes indicate exons of *Ctnnb1*. (**F**) Truncated β-catenin proteins in the liver tumors. All the tumors that were examined contained truncated β-catenin protein. The tumors overexpressed glutamine synthetase, consistent with the results of the immunohistochemistry analysis. (**G**) RT–PCR analysis of *Cre* transgene expression in liver tumors. Most of the tumors and all non-neoplastic liver tissues obtained from *Alb-Cre;Ctnnb1*$^{flox/flox}$ mice-retained *Cre* expression, but one tumor sample showed significantly reduced *Cre* expression. *Gusb* served as a positive control for the RT reactions. RT−, RNA samples without RT reactions served as negative controls; Control, control *Ctnnb1*$^{flox/flox}$ mice; M, DNA size marker; T, tumor; N, non-neoplastic liver tissue.

active in mature hepatocytes. As we previously reported, the efficient deletion of the conditional allele was also achieved in adult mice when crossed with *Ctnnb1*$^{flox/flox}$ mice. However, the present study showed that the efficient deletion was not maintained in elderly mice because of repopulation with wild-type hepatocytes that had escaped Cre-mediated recombination. Indeed, we previously reported a similar repopulation process in *Alb-Cre;Dicer*$^{flox/flox}$ mice although the repopulation took place at a much earlier time point (12). Our previous and present observations imply that repopulation with wild-type hepatocytes might not be an exceptional event and might represent a potential artifact in the analysis of hepatocyte-specific knockout mouse models.

Liver repopulation is a process in which a small number of phenotypically distinct hepatocytes gradually expand and replace the host hepatocytes *in vivo* (22,23). This phenomenon has been well documented in therapeutic liver repopulation, where wild-type hepatocytes are transplanted into metabolically defective livers and gradually replace the host hepatocytes (24). Because of the enormous proliferative capacity of hepatocytes, the introduction of a small number of wild-type hepatocytes is sufficient to repopulate a significant proportion of the mutant livers over time. This process takes place when the transplanted hepatocytes exhibit a growth advantage and continuous damage is occurring to the host hepatocytes.

Interestingly, wild-type hepatocytes predominantly replaced the pericentral areas, whereas β-catenin-deficient hepatocytes persistently resided in the periportal areas within the liver lobules of elderly *Alb-Cre;Ctnnb1*$^{flox/flox}$ mice. Wnt/β-catenin signaling is physiologically active in pericentral, but not periportal, hepatocytes (9,25). Accordingly, in the pericentral areas, the retention of β-catenin allows the proper transduction of Wnt/β-catenin signaling in wild-type hepatocytes, although Wnt/β-catenin signaling is blocked in β-catenin-deficient hepatocytes. As a result, wild-type hepatocytes selectively achieve the proper expression of β-catenin target genes and exhibit a survival advantage over β-catenin-deficient hepatocytes, as demonstrated in the present study. On the other hand, periportal hepatocytes do not express β-catenin target genes regardless of the status of the *Ctnnb1* alleles. Thus, wild-type hepatocytes are phenotypically indifferent from β-catenin-deficient hepatocytes in the periportal areas and do not exhibit a growth advantage.

Recent studies have shown the involvement of Wnt/β-catenin signaling in zonal gene expression within the liver lobule (25,26). Many β-catenin-regulated genes are related to the metabolic functions of hepatocytes; consequently, the region-specific activation of Wnt/β-catenin signaling is thought to be the basis for the metabolic heterogeneity of hepatocytes (25). In addition, the present observation implies that intact Wnt/β-catenin signaling confers a survival advantage to pericentral hepatocytes but not to periportal hepatocytes. Any of the β-catenin-regulated genes may be responsible for the survival advantage, but the exact mechanism remains to be elucidated.

Recently, Braeuning *et al.* (16) reported the presence of residual β-catenin-positive hepatocytes in young adult *Alb-Cre;Ctnnb1*$^{flox/flox}$ mice, consistent with our observation. A potentially discrepant finding is that the residual β-catenin-positive hepatocytes did not exhibit a growth advantage over β-catenin-deficient hepatocytes unless the mice were subjected to phenobarbital treatment. However, they examined mice that were up to 5 months old and that had been raised under normal breeding conditions. Indeed, in our gene expression analysis as well, 4-month-old mice exhibited no significant increases in the expressions of *Ctnnb1* and *Glul*, compared with the levels of 2-month-old mice. The expansion of the β-catenin-expressing hepatocytes became more obvious in elderly mice. Furthermore, the increased expression of Ki-67 further supports the growth advantage of β-catenin-positive hepatocytes over β-catenin-deficient hepatocytes.

At a glance, the spontaneous tumor development in 'β-catenin-deficient' livers seems paradoxical, since β-catenin is a major oncogene product. However, immunohistochemical and mutational analyses have revealed that these tumors did not actually lose β-catenin expression but rather acquired oncogenic mutations in their *Ctnnb1* alleles. Notably, the mutational analysis showed a characteristic mutation spectrum for the hepatomas that developed in *Alb-Cre;Ctnnb1*$^{flox/flox}$ mice. A significant proportion of the identified deletions involved loxP sites, and most of the tumors retained the expression of the *Cre* transgene. These observations suggest that these mutations were probably caused by the misrecombination of the loxP-flanked region. It might be possible that expression of Cre recombinase might be also responsible for the other mutations since the spectrum of *Ctnnb1* mutations in the current model is quite distinct from that of previously reported spontaneous mutations. All the mutations identified here were deletion mutations, whereas missense mutations are more common among spontaneous *Ctnnb1* mutations in mouse models of hepatocarcinogenesis (7,27). Indeed, illegitimate recombination arising from the transgenic expression of Cre or CreER^{T2} has been reported in some models in the absence of loxP-flanked conditional alleles (28,29). On the other hand, there were three tumors that showed significant reduction of *Cre* transgene expression. These tumors could be developed by acquisition of *Ctnnb1* mutations in β-catenin-positive hepatocytes that were escaped from *Cre*-mediated recombination although it is not a major pathway of tumorigenesis in this model.

The introduction of mutant β-catenin to hepatocytes is not sufficient to induce hepatocyte proliferation or to initiate tumorigenesis by itself in wild-type mice (30,31). Therefore, some factor promoting tumorigenesis probably exists in this model. Indeed, the process of liver repopulation has been suggested to increase the risk of tumorigenesis in several mouse models (32,33). The repopulation process allows the sustained clonal expansion of wild-type hepatocytes as well as hepatocytes with oncogenic alterations (34), and this process probably increases the risk of tumor progression (Figure 6). Together, these findings suggest that the concurrent occurrence of misrecombination and liver repopulation by wild-type hepatocytes resulted in tumorigenesis in the *Alb-Cre;Ctnnb1*$^{flox/flox}$ mice.

A recent study has reported an increase in tumor formation in *Alb-Cre;Ctnnb1*$^{flox/flox}$ mice treated with *N*-nitrosodiethylamine (35). However, the present study showed that *Alb-Cre;Ctnnb1*$^{flox/flox}$ mice actually develop liver tumors even in the absence of carcinogen treatment. Indeed, Rignall (36) reported that two of six tumors in *Alb-Cre;Ctnnb1*$^{flox/flox}$ mice treated by *N*-nitrosodiethylamine and phenobarbital exhibited *Ctnnb1* mutations. Of note, the authors only performed analysis of exon 3 of *Ctnnb1*, which would not have identified most of the large deletion mutations detected in our analysis. The potential occurrence of illegitimate recombination involving *Ctnnb1* and secondary effects by liver repopulation should be taken into consideration to accurately evaluate the effect of β-catenin-loss on hepatocarcinogenesis using this mouse model.

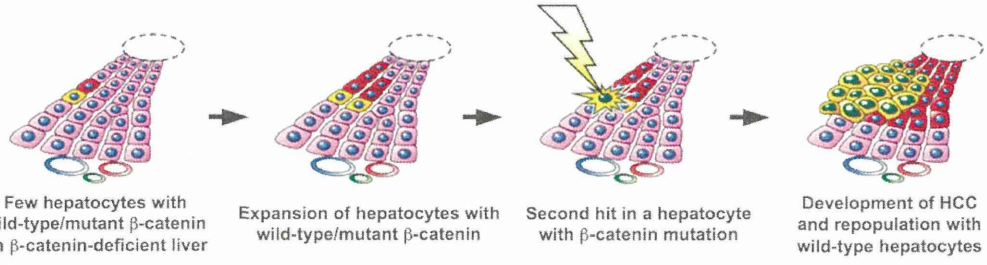

Fig. 6. Model of tumorigenesis in *Alb-Cre;Ctnnb1*$^{flox/flox}$ mouse livers At 2 weeks of age, the *Alb-Cre;Ctnnb1*$^{flox/flox}$ mouse livers are mostly composed of β-catenin-deficient hepatocytes (pink cells); however, a few residual β-catenin-positive hepatocytes that have escaped Cre-mediated recombination (red cells) and hepatocytes with activating *Ctnnb1* mutations as a result of illegitimate recombination (yellow cells) are present. Hepatocytes with wild-type or mutant β-catenin exhibit a survival advantage and gradually repopulate the pericentral areas. During this process, a 'second-hit', presumably an additional genetic alteration, initiates tumorigenesis in co-operation with the *Ctnnb1* mutation.

The present model probably represents an extreme example of artifacts related to the Cre-loxP system. However, the potential occurrence of repopulation should always be considered when analysing results obtained using hepatocyte-specific conditional knockout mouse models, particularly when mice of different ages are compared. Also, the formation of biologically active deletion mutants, such as dominant negative or constitutively active products, should be recognized as a potential adverse effect arising from illegitimate recombination in a manner that is not limited to the current model. Additionally, our findings demonstrated that active Wnt/β-catenin signaling confers a survival advantage to pericentral hepatocytes but not to periportal hepatocytes. Wnt/β-catenin signaling might act as a region-specific survival signal within the liver lobule.

Supplementary material

Supplementary Tables 1–3 can be found at http://carcin.oxfordjournals.org/

Funding

Takeda Science Foundation; KAKENHI (20790315) from the Ministry of Education, Culture, Sports, Science and Technology, Japan.

Acknowledgements

The authors thank Mr Shigeru Tamura for photographic assistance.

Conflict of Interest Statement: None declared.

References

1. Garcia-Otin,A.L. *et al.* (2006) Mammalian genome targeting using site-specific recombinases. *Front. Biosci.*, **11**, 1108–1136.
2. Branda,C.S. *et al.* (2004) Talking about a revolution: the impact of site-specific recombinases on genetic analyses in mice. *Dev. Cell*, **6**, 7–28.
3. Postic,C. *et al.* (2000) DNA excision in liver by an albumin-Cre transgene occurs progressively with age. *Genesis*, **26**, 149–150.
4. Postic,C. *et al.* (1999) Dual roles for glucokinase in glucose homeostasis as determined by liver and pancreatic beta cell-specific gene knock-outs using Cre recombinase. *J. Biol. Chem.*, **274**, 305–315.
5. Gordon,M.D. *et al.* (2006) Wnt signaling: multiple pathways, multiple receptors, and multiple transcription factors. *J. Biol. Chem.*, **281**, 22429–22433.
6. Morin,P.J. *et al.* (1997) Activation of beta-catenin-Tcf signaling in colon cancer by mutations in beta-catenin or APC. *Science*, **275**, 1787–1790.
7. de La Coste,A. *et al.* (1998) Somatic mutations of the beta-catenin gene are frequent in mouse and human hepatocellular carcinomas. *Proc. Natl Acad. Sci. USA*, **95**, 8847–8851.
8. Miyoshi,Y. *et al.* (1998) Activation of the beta-catenin gene in primary hepatocellular carcinomas by somatic alterations involving exon 3. *Cancer Res.*, **58**, 2524–2527.
9. Sekine,S. *et al.* (2007) Liver-specific loss of beta-catenin results in delayed hepatocyte proliferation after partial hepatectomy. *Hepatology*, **45**, 361–368.
10. Sekine,S. *et al.* (2006) Liver-specific loss of beta-catenin blocks glutamine synthesis pathway activity and cytochrome p450 expression in mice. *Hepatology*, **43**, 817–825.
11. Brault,V. *et al.* (2001) Inactivation of the beta-catenin gene by Wnt1-Cre-mediated deletion results in dramatic brain malformation and failure of craniofacial development. *Development*, **128**, 1253–1264.
12. Sekine,S. *et al.* (2009) Disruption of Dicer1 induces dysregulated fetal gene expression and promotes hepatocarcinogenesis. *Gastroenterology*, **136**, 2304–2315.
13. Sekine,S. *et al.* (2009) Dicer is required for proper liver zonation. *J. Pathol.*, **219**, 365–372.
14. Nakane,P.K. (1968) Simultaneous localization of multiple tissue antigens using the peroxidase-labeled antibody method: a study on pituitary glands of the rat. *J. Histochem. Cytochem.*, **16**, 557–560.
15. Sekine,S. *et al.* (2009) Esophageal melanomas harbor frequent NRAS mutations unlike melanomas of other mucosal sites. *Virchows Arch.*, **454**, 513–517.
16. Braeuning,A. *et al.* (2010) Phenotype and growth behavior of residual beta-catenin-positive hepatocytes in livers of beta-catenin-deficient mice. *Histochem. Cell Biol.*, **134**, 469–481.
17. Ward,J.M. *et al.* (1979) Neoplastic and nonneoplastic lesions in aging (C57BL/6N x C3H/HeN)F1 (B6C3F1) mice. *J. Natl Cancer Inst.*, **63**, 849–854.
18. Loeppen,S. *et al.* (2002) Overexpression of glutamine synthetase is associated with beta-catenin-mutations in mouse liver tumors during promotion of hepatocarcinogenesis by phenobarbital. *Cancer Res.*, **62**, 5685–5688.
19. Cadoret,A. *et al.* (2002) New targets of beta-catenin signaling in the liver are involved in the glutamine metabolism. *Oncogene*, **21**, 8293–8301.
20. Aydinlik,H. *et al.* (2001) Selective pressure during tumor promotion by phenobarbital leads to clonal outgrowth of beta-catenin-mutated mouse liver tumors. *Oncogene*, **20**, 7812–7816.
21. Loeppen,S. *et al.* (2005) A beta-catenin-dependent pathway regulates expression of cytochrome P450 isoforms in mouse liver tumors. *Carcinogenesis*, **26**, 239–248.
22. Sandgren,E.P. *et al.* (1991) Complete hepatic regeneration after somatic deletion of an albumin-plasminogen activator transgene. *Cell*, **66**, 245–256.
23. Overturf,K. *et al.* (1996) Hepatocytes corrected by gene therapy are selected in vivo in a murine model of hereditary tyrosinaemia type I. *Nat. Genet.*, **12**, 266–273.
24. Grompe,M. *et al.* (1999) Principles of therapeutic liver repopulation. *Semin. Liver Dis.*, **19**, 7–14.
25. Benhamouche,S. *et al.* (2006) Apc tumor suppressor gene is the "zonation-keeper" of mouse liver. *Dev. Cell*, **10**, 759–770.
26. Hailfinger,S. *et al.* (2006) Zonal gene expression in murine liver: lessons from tumors. *Hepatology*, **43**, 407–414.
27. Calvisi,D.F. *et al.* (2001) Activation of beta-catenin during hepatocarcinogenesis in transgenic mouse models: relationship to phenotype and tumor grade. *Cancer Res.*, **61**, 2085–2091.
28. Schmidt,E.E. *et al.* (2000) Illegitimate Cre-dependent chromosome rearrangements in transgenic mouse spermatids. *Proc. Natl Acad. Sci. USA*, **97**, 13702–13707.
29. Higashi,A.Y. *et al.* (2009) Direct hematological toxicity and illegitimate chromosomal recombination caused by the systemic activation of CreERT2. *J. Immunol.*, **182**, 5633–5640.
30. Harada,N. *et al.* (2002) Lack of tumorigenesis in the mouse liver after adenovirus-mediated expression of a dominant stable mutant of beta-catenin. *Cancer Res.*, **62**, 1971–1977.
31. Tward,A.D. *et al.* (2007) Distinct pathways of genomic progression to benign and malignant tumors of the liver. *Proc. Natl Acad. Sci. USA*, **104**, 14771–14776.
32. Sandgren,E.P. *et al.* (1992) DNA rearrangement causes hepatocarcinogenesis in albumin-plasminogen activator transgenic mice. *Proc. Natl Acad. Sci. USA*, **89**, 11523–11527.
33. Grompe,M. *et al.* (1998) Therapeutic trials in the murine model of hereditary tyrosinaemia type I: a progress report. *J. Inherit. Metab. Dis.*, **21**, 518–531.
34. Marongiu,F. *et al.* (2008) Liver repopulation and carcinogenesis: two sides of the same coin? *Am. J. Pathol.*, **172**, 857–864.
35. Zhang,X.F. *et al.* (2010) Conditional beta-catenin loss in mice promotes chemical hepatocarcinogenesis: role of oxidative stress and platelet-derived growth factor receptor alpha/phosphoinositide 3-kinase signaling. *Hepatology*, **52**, 954–965.
36. Rignall,B. *et al.* (2010) Tumor formation in liver of conditional {beta}-catenin-deficient mice exposed to a diethylnitrosamine / phenobarbital tumor promotion regimen. *Carcinogenesis*, **32**, 52–57.

Received November 19, 2010; revised December 22, 2010; accepted December 30, 2010